Inorg. Chem. **2005**, *44*, 1238–1247

Dioxygen Reactivity of Copper and Heme–Copper Complexes Possessing an Imidazole–Phenol Cross-Link

Eunsuk Kim,[†] Kaliappan Kamaraj,[†] Benedikt Galliker,[‡] Nick D. Rubie,[§] Pierre Moënne-Loccoz,[§] Susan Kaderli,[‡] Andreas D. Zuberbühler,[‡] and Kenneth D. Karlin*[,†]

Department of Chemistry, Johns Hopkins University, Baltimore, Maryland 21218, Department of Chemistry, University of Basel, Switzerland, and Department of Environmental and Biomolecular Systems, OGI School of Science and Engineering at Oregon Health & Science University (OHSU), Beaverton, Oregon 97006

Received August 9, 2004

Recent spectroscopic, kinetics, and structural studies on cytochrome *c* oxidases (C*c*Os) suggest that the histidine–tyrosine cross-link at the heme a_3–Cu_B binuclear active site plays a key role in the reductive O_2-cleavage process. In this report, we describe dioxygen reactivity of copper and heme/Cu assemblies in which the imidazole–phenol moieties are employed as a part of copper ligand $L^{N4}OH$ (2-{4-[2-(bis-pyridin-2-ylmethyl-amino)-ethyl]-imidazol-1-yl}-4,6-di -*tert*-butyl-phenol). Stopped-flow kinetic studies reveal that low-temperature oxygenation of $[Cu^{I}(L^{N4}OH)]^{+}$ (**1**) leads to rapid formation of a copper-superoxo species $[Cu^{II}(L^{N4}OH)(O_2^{-})]^{+}$ (**1a**), which further reacts with **1** to form the 2:1 Cu:O_2 adduct, peroxo complex $[\{Cu^{II}(L^{N4}OH)\}_2(O_2^{2-})]^{2+}$ (**1b**). Complex **1b** is also short-lived, and a dimer Cu(II)–phenolate complex $[Cu^{II}(L^{N4}O^{-})]_2^{2+}$ (**1c**) eventually forms as a final product in the later stage of the oxygenation reaction. Dioxygen reactivities of **1** and its anisole analogue $[Cu^{I}(L^{N4}OMe)]^{+}$ (**2**) in the presence of a heme complex $(F_8)Fe^{II}$ (**3**) (F_8 = tetrakis(2,6,-difluorotetraphenyl)-porphyrinate) are also described. Spectroscopic investigations including UV–vis, ^1H and ^2H NMR, EPR, and resonance Raman spectroscopies along with spectrophotometric titration reveal that low-temperature oxygenation of **1/3** leads to formation of a heme–peroxo–copper species $[(F_8)Fe^{III}–(O_2^{2-})–Cu^{II}(L^{N4}OH)]^{+}$ (**4**), $\nu_{(O-O)} = 813\ cm^{-1}$. Complex **4** is an S = 2 spin system with strong antiferromagnetic coupling between high-spin iron(III) and copper(II) through a bridging peroxide ligand. A very similar complex $[(F_8)Fe^{III}–(O_2^{2-})–Cu^{II}(L^{N4}OMe)]^{+}$ (**5**) ($\nu_{(O-O)} = 815\ cm^{-1}$) can be generated by utilizing the anisole compound **2**, which indicates that the cross-linked phenol moiety in **4** does not interact with the bridging peroxo group between heme and copper. This investigation thus reveals that a stable heme–peroxo–copper species can be generated even in the presence of an imidazole–phenol group (i.e., possible electron/proton donor source) in close proximity. Future studies are needed to probe key factors that can trigger the reductive O–O cleavage in C*c*O model compounds.

Introduction

The role of a cross-linked imidazole−phenol group in the heme/Cu/O_2 reaction has been intensely discussed[1] since such a moiety was first identified in the active site of cytochrome *c* oxidase (C*c*O) in 1998.[2] As an important metalloenzyme of a respiratory chain in many aerobic organisms, C*c*O produces proton gradients across the mitochondrial membrane via the coupled catalysis of the reduction of O_2 to water.[1,3] Dioxygen binding and reduction occurs at a heterobinuclear site that is comprised of a heme a_3 and Cu_B in close proximity (Figure 1), where one copper histidine ligand

* Author to whom correspondence should be addressed. Address: Department Chemistry, Remsen Hall, Johns Hopkins University, 3400 N. Charles Street, Baltimore, MD 21218; e-mail: karlin@jhu.edu; fax: 410-516-7044; phone: 410-516-8027.
[†] The Johns Hopkins University.
[‡] University of Basel.
[§] Oregon Health & Science University .

(1) Kim, E.; Chufan, E. E.; Kamaraj, K.; Karlin, K. D. *Chem. Rev.* **2004**, *104*, 1077−1133.
(2) Yoshikawa, S.; Shinzawa-Itoh, K.; Nakashima, R.; Yaono, R.; Yamashita, E.; Inoue, N.; Yao, M.; Jei-Fei, M.; Libeu, C. P.; Mizushima, T.; Yamaguchi, H.; Tomizaki, T.; Tsukihara, T. *Science* **1998**, *280*, 1723−1729.
(3) Ferguson-Miller, S.; Babcock, G. T. *Chem. Rev.* **1996**, *96*, 2889−2907.

10.1021/ic048907b CCC: $30.25
Published on Web 02/12/2005

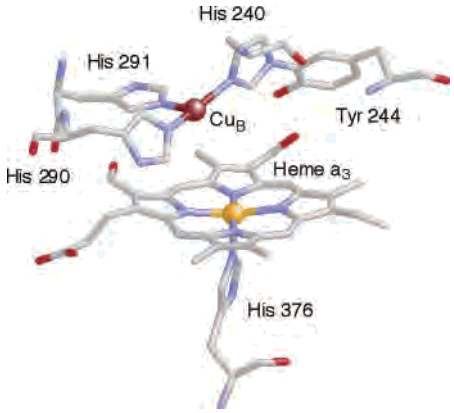

Figure 1. The reduced form of the heme a_3−Cu_B binuclear site from bovine cytochrome *c* oxidase.[2] The Fe^{II}...Cu^{I} distance is 5.2 Å. This figure was generated from Protein Data Bank coordinates (10CR) using the program Rasmol.

Scheme 1

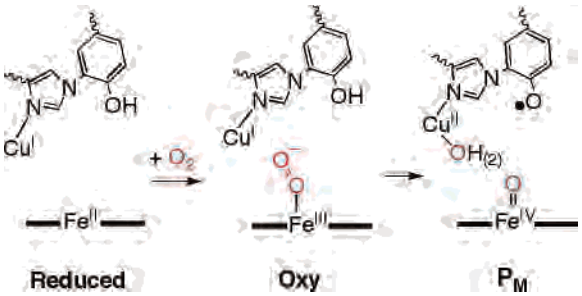

(H240) is covalently connected to a tyrosine side chain (Y244). The presence of this unique cross-link has further been supported by biochemical studies, and it is suggested to form through posttranslational modification.[1,4]

The O_2-reduction mechanism of C*c*O has been studied by various spectroscopic methods.[1,5] Although details of the reaction intermediates are not yet fully understood, there is a general agreement on certain aspects (Scheme 1).[1,6] When a mixed-valence C*c*O (i.e., the form in which only the heme a_3 and Cu_B are reduced, while the rest of the electron-transfer metal centers, Cu_A and heme *a*, remain oxidized) reacts with O_2, the O_2-binding occurs at heme a_3 to form an "oxy" intermediate (Scheme 1). Kinetic studies also suggest that there is an initial interaction between Cu_B and O_2 (not shown in Scheme 1) prior to formation of oxy.[1] The key O−O bond cleavage follows in the next step to yield an oxo ferryl (Fe^{IV}=O) species $\mathbf{P_M}$, where the cross-linked tyrosine is proposed to act as an electron/proton donor.[7−10] Such proposals triggered many chemists to model the imidazole−phenol cross-link to understand fundamental chemistry

Chart 1

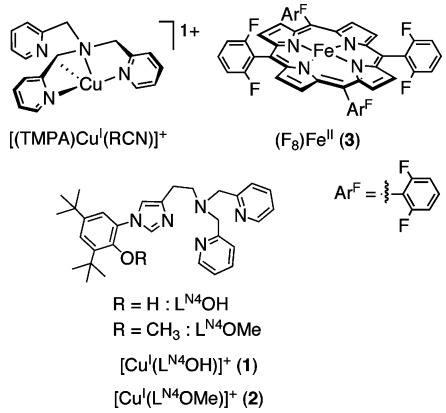

arising from this moiety. Because of its relatively recent discovery, most synthetic modeling studies have at this point been concerned with syntheses or physicochemical studies (e.g., pK_a, redox potential, or phenoxyl radical formation) of a simple imidazole−phenol organic compound without metal ions present.[11−19] There are only two reports on metal complexes possessing an imidazole−phenol cross-link, one of our own[20] and one from Naruta's[21] research group, which will be further discussed.

To gain fundamental insights into O_2-reduction chemistry in the C*c*O active site, we have been studying the dioxygen reactivity of a series of heme−copper assemblies.[22] In particular, Fe^{II}−Cu^{I} complexes with tris(2-pyridylmethyl)-amine (TMPA) and tetrakis(2,6,-difluorotetraphenyl)-porphyrinate (F_8) moieties (Chart 1) have been employed[23−26]

(4) Buse, G.; Soulimane, T.; Dewor, M.; Meyer, H. E.; Blüggel, M. *Prot. Sci.* **1999**, *8*, 985−990.
(5) Michel, H.; Behr, J.; Harrenga, A.; Kannt, A. *Annu. Rev. Biophys. Biomol. Struct.* **1998**, *27*, 329−356.
(6) Babcock, G. T. *Proc. Natl. Acad. Sci. U.S.A.* **1999**, *96*, 12971−12973.
(7) A nearby highly conserved tryptophan has also been discussed as a possible electron source.[8−10]
(8) Blomberg, M. R. A.; Siegbahn, P. E. M.; Wikström, M. *Inorg, Chem.* **2003**, *42*, 5231−5243.
(9) Siegbahn, P. E. M.; Blomberg, M. R. A. *Bba-Bioenergetics* **2004**, *1655*, 45−50.
(10) Svistunenko, D. A.; Wilson, M. T.; Cooper, C. E. *Bba-Bioenergetics* **2004**, *1655*, 372−380.
(11) McCauley, K. M.; Vrtis, J. M.; Dupont, J.; Van der Donk, W. A. *J. Am. Chem. Soc.* **2000**, *122*, 2403−2404.
(12) Cappuccio, J. A.; Ayala, I.; Elliott, G. I.; Szundi, I.; Lewis, J.; Konopelski, J. P.; Barry, B. A.; Einarsdottir, O. *J. Am. Chem. Soc.* **2002**, *124*, 1750−1760.
(13) Aki, M.; Ogura, T.; Naruta, Y.; Le, T. H.; Sato, T.; Kitagawa, T. *J. Phys. Chem. A* **2002**, *106*, 3436−3444.
(14) Collman, J. P.; Zhong, M. *Org. Lett.* **2000**, *2*, 1233−1236.
(15) Elliott, G. I.; Konopelski, J. P. *Org. Lett.* **2000**, *2*, 3055−3057.
(16) Naruta, Y.; Tachi, Y.; Chishiro, T.; Shimazaki, Y.; Tani, F. *Acta Crystallogr., Sect. E: Struct. Rep. Online* **2001**, *E57*, o550−o552.
(17) Tomson, F.; Bailey, J. A.; Gennis, R. B.; Unkefer, C. J.; Li, Z.; Silks, L. A.; Martinez, R. A.; Donohoe, R. J.; Dyer, R. B.; Woodruff, W. H. *Biochemistry* **2002**, *41*, 14383−14390.
(18) Collman, J. P.; Decreau, R. A.; Zhang, C. *J. Org. Chem.* **2004**, *69*, 3546−3549.
(19) Collman, J. P.; Decreau, R. A.; Costanzo, S. *Org. Lett.* **2004**, *6*, 1033−1036.
(20) Kamaraj, K.; Kim, E.; Galliker, B.; Zakharov, L. N.; Rheingold, A. L.; Zuberbuehler, A. D.; Karlin, K. D. *J. Am Chem. Soc.* **2003**, *125*, 6028−6029.
(21) Liu, J.-G.; Naruta, Y.; Tani, F.; Chishiro, T.; Tachi, Y. *Chem. Commun.* **2004**, 120−121.
(22) Karlin, K. D.; Kim, E. *Chem. Lett.* **2004**, *33*, 1226−1231.
(23) Ghiladi, R. A.; Hatwell, K. R.; Karlin, K. D.; Huang, H.-w.; Moënne-Loccoz, P.; Krebs, C.; Huynh, B. H.; Marzilli, L. A.; Cotter, R. J.; Kaderli, S.; Zuberbühler, A. D. *J. Am. Chem. Soc.* **2001**, *123*, 6183−6184.
(24) Chufán, E. E.; Karlin, K. D. *J. Am Chem. Soc.* **2003**, *125*, 16160−16161.
(25) Ghiladi, R. A.; Ju, T. D.; Lee, D.-H.; Moënne-Loccoz, P.; Kaderli, S.; Neuhold, Y.-M.; Zuberbühler, A. D.; Woods, A. S.; Cotter, R. J.; Karlin, K. D. *J. Am. Chem. Soc.* **1999**, *121*, 9885−9886.
(26) Ju, T. D.; Ghiladi, R. A.; Lee, D.-H.; van Strijdonck, G. P. F.; Woods, A. S.; Cotter, R. J.; Young, J., V. G.; Karlin, K. D. *Inorg. Chem.* **1999**, *38*, 2244−2245.

because the individual copper-only[27−29] or heme-only[30] O_2-chemistries with these ligands are very well understood. In light of the discovery of the His-Tyr cross-link in the C*c*O active site, we introduced an imidazole−phenol moiety to heme/Cu/O_2 chemistry by utilizing the ligand $L^{N4}OH$ (Chart 1) whose synthesis and initial copper-only O_2-reactivity were previously reported.[20] $L^{N4}OH$ and $L^{N4}OMe$ chelates are derivatives of TMPA, in which one of the pyridine arms is replaced with a cross-linked imidazole−phenol (or anisole) moiety (Chart 1).

In this report, additional studies and further kinetic/thermodynamic insights into the $[Cu^I(L^{N4}OH)]^+$ (**1**)/O_2 reaction are obtained using stopped-flow UV−vis spectroscopy. Then, we describe the chemistry of new heme−copper assemblies formed by dioxygen reactivity. $[Cu^I(L^{N4}OH)]^+$ (**1**)/$(F_8)Fe^{II}$ (**3**)/O_2 and $[Cu^I(L^{N4}OMe)]^+$ (**2**)/$(F_8)Fe^{II}$ (**3**)/O_2 produce heme−peroxo−copper species which have been characterized by low-temperature UV−vis, ^1H and ^2H NMR, and resonance Raman spectroscopies.

Experimental Section

Materials and Methods. All reagents and solvents were purchased from commercial sources and were of reagent quality unless otherwise stated. Air-sensitive compounds were handled under an argon atmosphere by using standard Schlenk techniques or in an MBraun Labmaster 130 inert atmosphere (<1 ppm O_2, <1 ppm H_2O) glovebox filled with nitrogen. Heptane and pentane were distilled over calcium hydride under argon, whereas acetonitrile (CH_3CN), dichloromethane (CH_2Cl_2), and tetrahydrofuran (THF) were purified over activated alumina columns under nitrogen. Deoxygenation of these solvents was achieved by bubbling with argon for 30 min and (followed) by three freeze/pump/thaw cycles prior to introduction into the glovebox.

Benchtop UV−vis experiments were carried out using a Hewlett-Packard 8453 diode array spectrometer equipped with HP Chemstation software, where the spectrometer was equipped with a variable-temperature Dewar and cuvette assembly, as described elsewhere.[31,32]

Synthesis. $[Cu^I(L^{N4}OH)]B(C_6F_5)_4$ (**1**),[20] $[Cu^I(L^{N4}OMe)]B(C_6F_5)_4$ (**2**),[20] $(F_8)Fe^{II}$ (**3**),[30,33] (both as solvates, see references 30, 33 and below) and $(F_8\text{-}d_8)Fe^{II}$ (**3-*d*$_8$**)[33] complexes were synthesized according to published procedures. The transient dioxygen adducts of copper complexes, $[Cu^{II}(L^{N4}OH)(O_2^{\cdot-})]^+$ (**1a**) and $[\{Cu^{II}(L^{N4}OH)\}_2(O_2^{2-})]^{2+}$ (**1b**), were generated by mixing dioxygen saturated solvent with a solution of $[Cu^I(L^{N4}OH)]^+$ (**1**) under nitrogen or argon in a stopped-flow instrument. The heme−peroxo−copper complexes $[(F_8)Fe^{III}-(O_2^{2-})-Cu^{II}(L^{N4}OH)]^+$ (**4**) and $[(F_8)Fe^{III}-(O_2^{2-})-Cu^{II}(L^{N4}OMe)]^+$ (**5**) were prepared in situ by bubbling cold (−40 to −80 °C) solutions of **1**/**3** or **2**/**3** with dry (passed through Drierite) O_2 gas from the tank.

Stopped-Flow Kinetics. Kinetics were followed on a Canterbury variable temperature stopped-flow unit (SF L-21 flow module with an SF-3L flow unit, Hi-Tech Scientific) with a 2-mm path length cell. The diode arrays used were a J & M TIDAS-MMS/16 VIS/500 diode array UV−vis spectrophotometer (256 diodes, 300−1100 nm, 0.8-ms integration time). A CLH 111 halogen lamp (ZEISS) was used as light source. THF (puriss, Fluka) was freshly distilled prior to use from an argon-saturated benzophenone/sodium still. Solutions of the copper complexes were prepared in an MBraun glovebox. Up to 250 complete spectra and up to four different time bases were used. Obtaining variable O_2 concentrations in solution was achieved with two MKS PR-4000 Mass-Flo-Controller-units. Detailed sampling information for each experiment (i.e., sample concentrations, time, temperature, etc) is presented in Table S1 (Supporting Information). In the present study, an updated value for the solubility of dioxygen in tetrahydrofuran (25 °C) has been employed for calculations, $[O_2] = 8.07 \times 10^{-3}$ M.[34] For numerical analysis, all kinetic runs were pretreated by factor analysis and analyzed globally. Concentration profiles and spectra of the individual species were calculated on the basis of different kinetic schemes using Specfit (Spectrum Software Ass.) by numerical integration of the appropriate set of differential equations. Equilibrium constants were obtained either kinetically from the respective rate constants of the forward and back reactions or (in rapid equilibria) directly from individual absorbance traces with the aid of independently determined species spectra. See also previous papers for examples of application of Specfit to kinetics of the type described here.[28]

Spectrophotometric Titration of a (1)/(3) Mixture with Dioxygen in the Formation of $[(F_8)Fe^{III}-(O_2^{2-})-Cu^{II}(L^{N4}OH)]^+$ (4). In the glovebox, a roughly 0.2−0.4 mM stock solution of a 1:1 mixture of $[Cu^I(L^{N4}OH)]^+$ (**1**) and $(F_8)Fe^{II}$ (**3**) was prepared. For example, 24 mg (0.0187 mmol) of **1**•0.3C_5H_{12}•0.3$C_4H_{10}O$ and 15 mg (0.0181 mmol) of **3**•H_2O were dissolved in 0.8 mL of THF. This solution was further diluted (roughly10-fold) and transferred to a 2-mm path length Schlenk cuvette. A UV−vis spectrum of the solution was recorded at −73 °C and the exact concentration of this diluted solution mixture of **1** and **3** was calculated from the extinction coefficient of $(F_8)Fe^{II}$ (**3**) that was separately determined. The cuvette was capped with a 14/24 adapter (purchased from Chemglass CG1036-14) whose opposite end was designed to fit a rubber septum. Two appropriate size rubber septa and a Teflon septum were used to seal the Schlenk cuvette from the atmosphere. The cuvette assembly was then transferred to the low-temperature UV−vis spectrometer and cooled to −73 °C. Separately, a 250-mL two sidearm Schlenk flask, whose neck was closed with a rubber septum and one sidearm was connected to an oil bubbler, was filled with 1.01% O_2 in Ar gas mixture (custom purchased from Potomac Airgas, Baltimore, MD) under 1 atm pressure. A Hamilton gastight syringe equipped with a three-way purge valve (for Ar purging of the syringe and the needle) was used to transfer specific amounts of the 1.01% O_2 gas to the cold solution of **1** and **3**. To the cuvette containing a solution of **1** and **3** were added 0.5 equiv, 1 equiv, and 2 equiv of dioxygen in three separate experiments. Each aliquot of dioxygen was bubbled directly into the solution via syringe and the resulting solution was allowed to react until no spectral change was observed in the UV−vis spectrum

(27) Karlin, K. D.; Kaderli, S.; Zuberbühler, A. D. *Acc. Chem. Res.* **1997**, *30*, 139−147.
(28) Zhang, C. X.; Kaderli, S.; Costas, M.; Kim, E.-i.; Neuhold, Y.-M.; Karlin, K. D.; Zuberbühler, A. D. *Inorg. Chem.* **2003**, *42*, 1807−1824.
(29) Fry, H. C.; Scaltrito, D. V.; Karlin, K. D.; Meyer, G. J. *J. Am Chem. Soc.* **2003**, *125*, 11866−11871.
(30) Ghiladi, R. A.; Kretzer, R. M.; Guzei, I.; Rheingold, A. L.; Neuhold, Y.-M.; Hatwell, K. R.; Zuberbühler, A. D.; Karlin, K. D. *Inorg. Chem.* **2001**, *40*, 5754−5767.
(31) Karlin, K. D.; Cruse, R. W.; Gultneh, Y.; Farooq, A.; Hayes, J. C.; Zubieta, J. *J. Am. Chem. Soc.* **1987**, *109*, 2668−2679.
(32) Karlin, K. D.; Haka, M. S.; Cruse, R. W.; Meyer, G. J.; Farooq, A.; Gultneh, Y.; Hayes, J. C.; Zubieta, J. *J. Am. Chem. Soc.* **1988**, *110*, 1196−1207.
(33) Kopf, M.-A.; Neuhold, Y.-M.; Zuberbühler, A. D.; Karlin, K. D. *Inorg. Chem.* **1999**, *38*, 3093−3102.
(34) Fischer, K.; Horstmann, S. Auftragsmessung im Laboratory for Thermophysical Properties GmbH der Universität Oldenburg, Oldenburg, Germany, 2003.

(typically, it took ∼36−48 h). Whereas about one-half the amount of reduced starting material **1**/**3** was present with addition of 0.5 equivalent O_2, full formation of $[(F_8)Fe^{III}-(O_2^{2-})-Cu^{II}(L^{N4}OH)]^+$ (**4**) was obtained with an additional 0.5 equivalent O_2 (thus, a total of one equivalent O_2), see Supporting Information, Figure S6. In a separate experiment with one equivalent O_2, ∼95% formation of **4** was observed. Therefore, the reaction stoichiometry of **1** and **3** to O_2 was concluded to be 1:1.

NMR Spectroscopy. ^{1}H NMR spectra at room temperature were recorded either on a Varian Unity 400 or on a Bruker 300 NMR instrument. Variable temperature and ^{2}H NMR spectroscopic studies were carried out on a Varian Unity 400 NMR instrument (^{1}H at 400 MHz, ^{2}H at 61 MHz). All spectra were recorded in 5-mm o.d. NMR tubes. The chemical shifts were reported as δ (ppm) values calibrated to natural abundance deuterium or proton solvent peaks. A tunable broadband probe was used in collecting ^{2}H NMR spectra. Typically, 16−23 mg of $[Cu^I(L^{N4}OH)]^+$ (**1**) or $[Cu^I(L^{N4}OMe)]^+$ (**2**) and 10−15 mg of $(F_8)Fe^{II}$ (**3**) or $(F_8$-$d_8)Fe^{II}$ (**3**-d_8) in ∼0.5 mL of proper solvent were used for each experiment.

Resonance Raman Spectroscopy. In the glovebox, 5 mM MeCN solutions of a mixture of $[Cu^I(L^{N4}OH)]^+$ (**1**) and $(F_8)Fe^{II}$ (**3**) or a mixture of $[Cu^I(L^{N4}OMe)]^+$ (**2**) and $(F_8)Fe^{II}$ (**3**) were prepared and transferred to NMR tubes (∼0.5 mL solution per tube) and capped with tight-fitting septa. The sample tubes were placed in a cold bath (dry ice/MeCN) for ∼15 min and oxygenated using $^{16}O_2$ and $^{18}O_2$ ($^{18}O_2$ gas was purchased from ICON, Summit, NJ, and $^{16}O_2$ gas was purchased from BOC gases, Murray Hill, NJ). The labeled gases were cooled in dry ice for 5 min and injected through the solution by using a Hamilton gastight syringe. The oxygenated samples were set in a cold bath for ∼10 min, after which the sample tubes were frozen in liquid N_2 and sealed by flame.

Resonance Raman spectra were collected on a McPherson 2061/207 spectrograph in a 0.67-m configuration equipped with a Kaiser Optical supernotch filter to minimize interferences from the Rayleigh scattering. Raman scattered light, gathered in a backscattering geometry, was dispersed using a 2400gr/mm holographic grating and analyzed using a liquid nitrogen cooled Princeton Instruments LN-1100PB CCD detector. A Coherent Innova 302 krypton ion laser was used as the source for the 413-nm excitation. The samples were placed in a custom glass Dewar equipped with a copper coldfinger cooled with liquid nitrogen to maintain the sample temperature at ∼90 K. A custom sample spinning was employed to minimize sample degradation upon laser illumination. Additionally, the laser power was kept below 10 mW and individual spectra were compared to confirm the integrity of the samples during the data acquisition. Vibration frequencies were calibrated relative to an internal standard and are accurate to ±1 cm^{-1}.

Electron Paramagnetic Resonance (EPR) Spectroscopy. The X-band EPR spectrum of $[(F_8)Fe^{III}-(O_2^{2-})-Cu^{II}(L^{N4}OH)]^+$ (**4**) was recorded on a Bruker EMX spectrometer, with temperature maintained at 77 K using a coldfinger filled with liquid nitrogen, through which gas helium was bubbled. In a glovebox, a THF solution (1 mM) of an equimolar mixture of **1** and **3** was prepared and transferred to an EPR tube. The tube was capped with a rubber septum and transferred to a −95 °C cold bath (N_2/hexane). Dry dioxygen was added through the solution via syringe to generate $[(F_8)Fe^{III}-(O_2^{2-})-Cu^{II}(L^{N4}OH)]^+$ (**4**). The resulting solution was allowed to sit at −95 °C for 10 min, after which the solution was frozen in liquid N_2.

Scheme 2

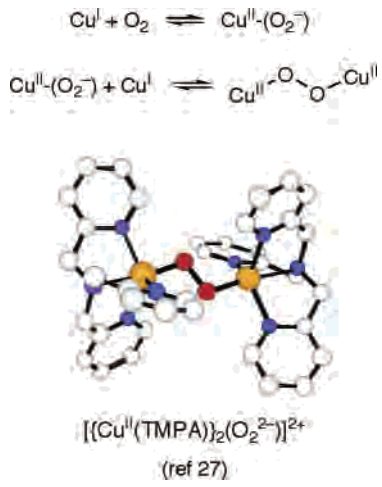

Results and Discussion

Interaction of $[Cu^I(L^{N4}OH)]B(C_6F_5)_4$ (1) with O_2. The kinetic and thermodynamic properties of the reaction of **1** with O_2 are of particular current interest within the field of copper−dioxygen reactivity, because of presence of the imidazole−phenol moiety in **1**. Kinetic studies on heme−copper oxidases suggest that O_2 equilibrates with the Cu_B center (with imidazole−phenol; see Introduction) prior to binding at heme a_3.[35−37]

Initial studies of Cu^I/O_2 reactions of $L^{N4}OMe$ and $L^{N4}OH$ were carried out by benchtop UV−vis spectroscopy. As previously noted,[20] the Cu^I/O_2 reaction with $L^{N4}OMe$ resembled that of TMPA; in the $[Cu^I(TMPA)(RCN)]^+/O_2$ reaction, oxygenation leads to the formation of a low-temperature stable μ-1,2 peroxo dicopper species, where stopped-flow studies revealed that an initial 1:1 adduct, $[(TMPA)Cu^{II}(O_2^-)]^+$, forms prior to formation of μ-1,2 peroxo complex (Scheme 2).[27] On the other hand, with the phenol analogue $[Cu^I(L^{N4}OH)]B(C_6F_5)_4$ (**1**) in benchtop experiments, we observed that the μ-1,2 peroxo species was only short-lived and it transformed to a phenolate dimeric complex $[Cu^{II}(L^{N4}O^-)]_2^{2+}$ (**1c**) even at −80 °C within a few minutes.[20] The fast **1**/O_2 reaction was further studied by UV−vis stopped-flow kinetics, and here we describe the results in comparison with those from the $[Cu^I(TMPA)(RCN)]^+/O_2$ reaction, that is, the closely related system without an imidazole−phenol moiety (Chart 1 and Scheme 2).

The kinetic scheme deduced for the reaction of $[Cu^I(L^{N4}OH)]^+$ (**1**) with dioxygen in THF is outlined in Scheme 3. In fact, the formation of dioxygen adducts of **1** follows the same mechanism which has been found in the analogous reaction of $[Cu^I(TMPA)(RCN)]^+/O_2$ (R = Me or Et).[28,38] At low temperatures, $[Cu^I(L^{N4}OH)]^+$ (**1**) (λ_{max} = 356 nm) reacts with dioxygen in a reversible fashion to form a 1:1 $Cu-O_2$ species, formulated as for related systems[28,38] as a superoxo−

(35) Oliveberg, M.; Malmström, B. G. *Biochemistry* **1992**, *31*, 3560−3563.
(36) Blackmore, R. S.; Greenwood, C.; Gibson, Q. H. *J. Biol. Chem.* **1991**, *266*, 19245−19249.
(37) Varotsis, C.; Zhang, Y.; Appelman, E. H.; Babcock, G. T. *Proc. Natl. Acad. Sci. U.S.A.* **1993**, *90*, 237−241.
(38) Karlin, K. D.; Wei, N.; Jung, B.; Kaderli, S.; Niklaus, P.; Zuberbühler, A. D. *J. Am Chem. Soc.* **1993**, *115*, 9506−9514.

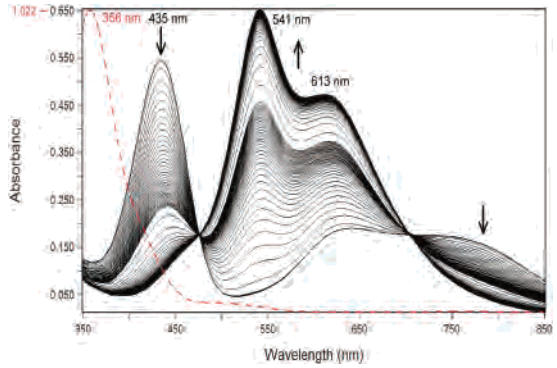

Figure 2. Time-dependent UV−vis spectra (136 s, total) for the oxygenation of $[Cu^{I}(L^{N4}OH)]^{+}$ (**1**) in THF at −105 °C. The spectrum of **1** (λ_{max} = 356 nm) is shown in red (dotted). Oxygenation gives intermediate formation of $[Cu^{II}(L^{N4}OH)(O_2^{-})]^{+}$ (**1a**) (λ_{max} = 435 nm, black) which decays to the peroxo complex $[\{Cu^{II}(L^{N4}OH)\}_2(O_2^{2-})]^{2+}$ (**1b**) (λ_{max} = 541, 613 nm, black).

Scheme 3

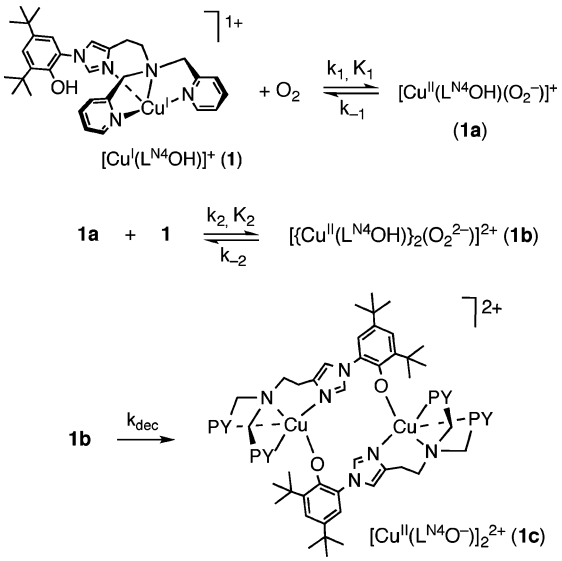

copper(II) complex $[Cu^{II}(L^{N4}OH)(O_2^{-})]^{+}$ (**1a**) (λ_{max} = 435 nm) with characteristic UV−vis spectral pattern;[39] this further reacts with another molecule of **1** to form a μ-1,2 dicopper peroxo species, $[\{Cu^{II}(L^{N4}OH)\}_2(O_2^{2-})]^{2+}$ (**1b**) with intense UV−vis features at 541 and 613 nm, Figure 2. Because of their short lifetimes, the assignments of **1a** and **1b** are primarily based on the kinetic behavior (vide infra) and distinctive UV−vis features, where the diagnostic[39] $\pi^* \rightarrow$ d superoxo to Cu(II) (435 nm) and $\pi^* \rightarrow$ d peroxo to Cu(II) (541 and 613 nm) charge-transfer transitions are seen (Figure 2). The formation of **1a** (λ_{max} = 435 nm) is extremely favorable and fast in the weakly coordinating solvent THF, and even at −105 °C it is complete within the mixing time (~1.3 ms). Only subsequent decay of **1a** was observed with concomitant or subsequent formation of **1b** (λ_{max} = 541 and 613 nm). The closely related complex $[(TMPA)Cu^{I}(RCN)]^{+}$ reacts similarly fast in THF;[28,29] in fact, using transient absorption laser flash photolysis of a carbonyl complex $[(TMPA)Cu^{I}(CO)]^{+}$ in the presence of CO and O_2, the second-order rate constant for formation of $[(TMPA)Cu^{I}(O_2^{-})]^{+}$ in THF was determined to be 1.3×10^9 M^{-1} s^{-1} at room temperature.[29]

(39) Mirica, L. M.; Ottenwaelder, X.; Stack, T. D. P. *Chem. Rev.* **2004**, *104*, 1013−1045.

Table 1. Thermodynamic Parameters for O_2-Binding to $[Cu^{I}(L^{N4}OH)]^{+}$ (**1**) and $[Cu^{I}(TMPA)(RCN)]^{+}$ in THF, Forming the 1:1 Superoxo−Copper(II) Complex $[(L)Cu^{II}(O_2^{-})]^{+}$

parameter	**1**	$[Cu^{I}(TMPA)(RCN)]^{+}$ [a]
K_1 (M^{-1}) at 183 K	$(5.28 \pm 0.05)\cdot 10^2$	$(6 \pm 2)\cdot 10^5$
223 K	$(1.01 \pm 0.01)\cdot 10^1$	$(4.5 \pm 0.4)\cdot 10^3$
$\Delta H°$ (kJ mol^{-1})	-33.6 ± 0.1	-41 ± 2
$\Delta S°$ (J K^{-1} mol^{-1})	-131.3 ± 0.7	-114 ± 7
reference	This Work	recalculated from ref 28

[a] Recalculated values from those used in ref 26, now using a new value for O_2 solubility in THF at 25 °C, $[O_2] = 8.07 \times 10^{-3}$ M.[34]

As mentioned, the rapid rate of formation of $[Cu^{II}(L^{N4}OH)(O_2^{-})]^{+}$ (**1a**) precluded determination of the rate constants for O_2-binding (k_1) and dissociation (k_{-1}). However, thermodynamic parameters could be extracted from the temperature dependence of the spectral changes (a Van't Hoff plot for K_1 is available in Supporting Information, Figure S1). As presented in Table 1, the general observation of superoxo−copper(II) formation with $L^{N4}OH$ has similarities to that with TMPA, where the stability of dioxygen binding to a copper(I) ion is controlled by favorable enthalpy but unfavorable entropy. Therefore, the spectrum of **1a** is better seen at lower temperatures (see Figure 2 and Figure S2 in Supporting Information). A striking difference in the thermodynamic binding constant K_1 is observed between **1a** and $[Cu^{II}(TMPA)(O_2^{-})]^{+}$, where the former is smaller by ~3 orders of magnitude (Table 1). This appears to be controlled primarily by significant differences in enthalpy. Previous kinetic and thermodynamic studies[28] on a series of $[Cu^{I}(R\text{-}TMPA)]^{+}$ complexes (R = H, Me−, *t*Bu−, MeO−, and Me_2N− substituents on the pyridine ring para-position) show that the electronic properties of copper complexes strongly affect kinetics and thermodynamics of their O_2-adducts (i.e., superoxo or peroxo species); more electron-rich ligand−copper (e.g., R = Me_2N−) complexes produce more thermally stable O_2-adducts with faster reaction rates. The $Cu^{II/I}$ redox potentials of **1**, **2**, and $[Cu^{I}(TMPA)(RCN)]^{+}$ were previously measured by cyclic voltammetry, and essentially identical values were obtained for all three complexes ($E_{1/2}$ = −0.42 V versus $FeCp_2/FeCp_2^{+}$ in MeCN).[20] This suggests that electronic influences are probably not significant and the weaker complex formation observed for **1a** would seem to originate from steric influences inherent in the $L^{N4}OH$ ligand and copper complex architecture. Whether this is related to the phenol−imidazole cross-link or with the inherent properties caused by an ethyl imidazole chelate (i.e., N−CH_2CH_2−imidazolyl) versus a methylpyridyl group (i.e., N−CH_2−pyridyl in TMPA) is not clear.

Formation of μ-peroxo binuclear complex $[\{Cu^{II}(L^{N4}OH)\}_2(O_2^{2-})]^{2+}$ (**1b**) also derives from a reversible reaction of $[Cu^{II}(L^{N4}OH)(O_2^{-})]^{+}$ (**1a**) and $[Cu^{I}(L^{N4}OH)]^{+}$ (**1**), which can be described by the rate and equilibrium constants k_2, k_{-2}, and K_2 (Scheme 3 and Table 2). These parameters are reasonably defined but estimated errors are somewhat larger

Table 2. Kinetic and Thermodynamic Parameters for Formation of the Peroxo Species $[\{Cu^{II}(L)\}_2(O_2^{2-})]^{2+}$ from the Reaction of $[(L)Cu^{II}(O_2^{-})]^{+}$ and $[(L)Cu^{I}]^{+}$ in THF, where L = $L^{N4}OH$ or TMPA. See Scheme 3

parameter	$[\{Cu^{II}(L^{N4}OH)\}_2(O_2^{2-})]^{2+}$ (**1b**)	$[\{Cu^{II}(TMPA)\}_2(O_2^{2-})]^{2+}$ [a]
k_2 ($M^{-1}s^{-1}$) at 168 K	$(7.3 \pm 0.4)\cdot10^3$	$(3.30 \pm 0.08)\cdot10^4$
238 K	$(1.2 \pm 0.1)\cdot10^6$	$(1.84 \pm 0.02)\cdot10^6$
$\Delta H^{\ddagger}$ (kJ mol^{-1})	22.6 ± 0.6	17.4 ± 0.1
$\Delta S^{\ddagger}$ (J K^{-1} mol^{-1})	-32 ± 3	-49.8 ± 0.6
k_{-2} (s^{-1}) at 213 K	$(9.5 \pm 0.6)\cdot10^{-1}$	$(1.4 \pm 0.9)\cdot10^{-3}$
238 K	$(4.1 \pm 0.3)\cdot10^1$	$(1.0 \pm 0.3)\cdot10^{-1}$
$\Delta H^{\ddagger}$ (kJ mol^{-1})	61 ± 2	70 ± 4
$\Delta S^{\ddagger}$ (J K^{-1} mol^{-1})	46 ± 9	32 ± 14
K_2 (M^{-1}) at 183 K	$(1.1 \pm 0.3)\cdot10^7$	$5\cdot10^{10}$ [b]
223 K	$(1.11 \pm 0.09)\cdot10^5$	$(1.1\pm 0.5)\cdot10^8$
$\Delta H°$ (kJ mol^{-1})	-39 ± 2	-53 ± 4
$\Delta S°$ (J K^{-1} mol^{-1})	-78 ± 10	-82 ± 14
K_{on} (M^{-2}) at 183 K	$(6 \pm 2)\cdot10^9$	$5\cdot10^{16}$ [a]
223 K	$(1.12 \pm 0.09)\cdot10^6$	$(5 \pm 2)\cdot10^{11}$
$\Delta H°$ (kJ mol^{-1})	-72 ± 2	-93 ± 3
$\Delta S°$ (J K^{-1} mol^{-1})	-209 ± 10	-195 ± 9
reference	This Work	recalculated from ref 28

[a] Corrected values from those used in ref 26, now using a new value for O_2 solubility in THF at 25 °C, $[O_2] = 8.07 \times 10^{-3}$ M.[34] [b] Strongly extrapolated value with high uncertainty.

than for other systems,[27,28,40] because of the limited temperature range amenable to analysis. These parameters were determined on the basis of the rate law derived from Scheme 3. K_1 was kept fixed at values calculated from the thermodynamic parameters collected in Table 1 while k_2 and k_{-2} (and if necessary k_{dec}) were the adjustable parameters. At medium temperatures, up to about −30 °C, complications in the analyses arose, indicating the presence of additional species, beyond those indicated in Scheme 3.[41] Nevertheless, trends and data obtained reveal that **1b** has similar k_2 values to those determined for $[\{Cu^{II}(TMPA)\}_2(O_2^{2-})]^{2+}$,[28] but it has considerably larger k_{-2} values (by ∼2 orders of magnitude), Table 2. Since the back reaction (i.e., k_{-2} process) pertains to the Cu−O bond breaking, the more favorable activation enthalpy for this reverse reaction found for $[\{Cu^{II}(L^{N4}OH)\}_2(O_2^{2-})]^{2+}$ (**1b**) may reflect its less favorable peroxo structure, compared to that of $[\{Cu^{II}(TMPA)\}_2(O_2^{2-})]^{2+}$. The overall thermodynamic properties, that is, those estimated for K_2, K_{on} ($=K_1 \times K_2$), and $\Delta H°$ (Table 2), also support the view that $[\{Cu^{II}(L^{N4}OH)\}_2(O_2^{2-})]^{2+}$ (**1b**) is less thermodynamically stable than $[\{Cu^{II}(TMPA)\}_2(O_2^{2-})]^{2+}$.

In the later stage of the oxygenation reaction, the cross-linked phenol acts as a proton donor to form a Cu(II)−phenolate complex $[Cu^{II}(L^{N4}O^{-})]_2^{2+}$ (**1c**) (Scheme 3).[20] This is parallel to the reactions of $[\{Cu^{II}(TMPA)\}_2(O_2^{2-})]^{2+}$ with 2,4-di-*tert*-buthylphenol or HPF_6,[42] where the phenol, as an acid, protonates the peroxide to generate H_2O_2, leaving a phenolate and copper(II) species. Thus, during the decomposition process of $[\{Cu^{II}(L^{N4}OH)\}_2(O_2^{2-})]^{2+}$ (**1b**) to

Scheme 4

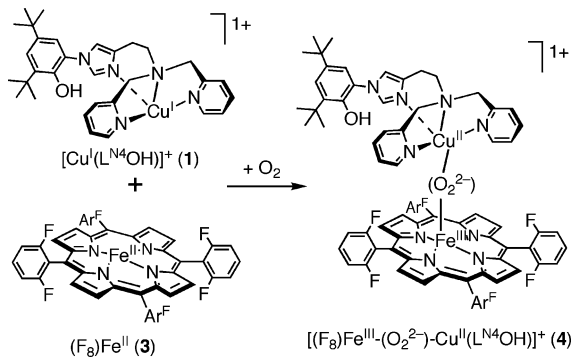

$[Cu^{II}(L^{N4}O^{-})]_2^{2+}$ (**1c**), H_2O_2 is presumed to form.[43] Although the dimeric structure of **1c** (Scheme 3) would not be relevant to C*c*O active site chemistry, the aspect of the phenol moiety being a H^+ source could be important because the O−O reductive cleavage at heme a_3/Cu_B requires protons.[44] The kinetic studies on the formation of **1c** were carried out in the temperature range of −25 °C to +25 °C using k_{HT} in a simplified model to fit the data: 2 $[Cu^{I}(L^{N4}OH)]^{+}$ (**1**) + O_2 → $[Cu^{II}(L^{N4}O^{-})]_2^{2+}$ (**1c**). As shown in Figure S3 (Supporting Information), there is a steady formation of the purple phenolate copper(II) dimeric product **1c** ($\lambda_{max} = 518$ and 793 nm) whose process can be analyzed by $\Delta H^{\ddagger}$ (kJ mol^{-1}) = -41.0 ± 0.9 and $\Delta S^{\ddagger}$ (J $K^{-1}mol^{-1}$) = -328 ± 3 (an Eyring plot is also available in Supporting Information, Figure S4). Obviously, the above reaction is *not* an elementary step but is composed of a series of left-lying equilibria including the species $[Cu^{II}(L^{N4}OH)(O_2^{-})]^{+}$ (**1a**) and $[\{Cu^{II}(L^{N4}OH)\}_2(O_2^{2-})]^{2+}$ (**1b**), observed at lower temperatures. Only by the combination of such preequilibria can the observed strongly negative activation parameters be rationalized.

Oxygenation of Heme/Copper Assemblies. With known independent O_2-chemistry for $[Cu^{I}(L^{N4}OH)]^{+}$ (**1**) and (F_8)-Fe^{II} (**3**) (Chart 1),[30] we studied the oxygenation reaction of equimolar mixtures of **1** and **3**. This self-assembly approach in heme/Cu^{I}/O_2 reactivity studies was successfully used in the past, yielding discrete heme−peroxo−copper complexes without forming heme-only or copper-only O_2-products.[1,23] This method has some advantage over a heterobinuclear system which requires more demanding ligand syntheses and can lead to more complicated spectroscopic features. Here, in the reactions of **1**/**3**/O_2, a new high-spin heme−peroxo−copper complex $[(F_8)Fe^{III}-(O_2^{2-})-Cu^{II}(L^{N4}OH)]^{+}$ (**4**) is generated (Scheme 4).

This current study complements investigations with related systems, $[Cu^{I}(TMPA)(RCN)]^{+}$/$(F_8)Fe^{II}$ (**3**)/O_2 (Chart 1)[23] and $[(L^{OH})Fe^{II}Cu^{I}]^{+}$/$O_2$ (from Naruta's group, see diagram);[21] the former represents a reaction quite analogous to **1**/**3**/O_2 but it does not contain the imidazole−phenol moiety, while the latter is a binuclear system which has a covalently attached

(40) Liang, H.-C.; Karlin, K. D.; Dyson, R.; Kaderli, S.; Jung, B.; Zuberbühler, A. D. *Inorg. Chem.* **2000**, *39*, 5884−5894.
(41) In fact, we cannot be sure whether **1c** forms directly from **1b** or rather from another species in equilibrium with **1b**.
(42) Paul, P. P.; Tyeklár, Z.; Jacobson, R. R.; Karlin, K. D. *J. Am. Chem. Soc.* **1991**, *113*, 5322−5332.
(43) Chemical tests (e.g., with a titanium reagent) for hydrogen peroxide were negative, but we separately observed that $[Cu^{II}(L^{N4}O^{-})]_2^{2+}$ (**1c**) effected decomposition of H_2O_2.

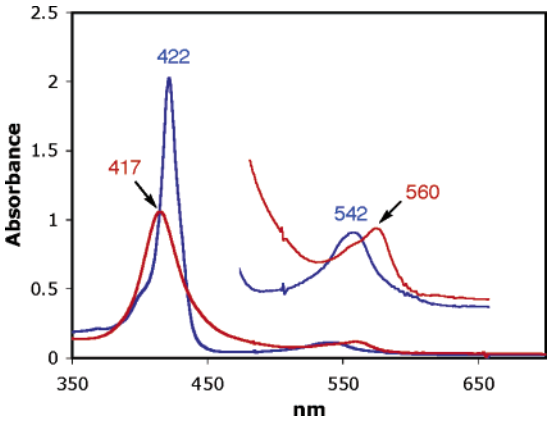

Figure 3. UV-visible spectra of the oxygenation reaction of $[Cu^{I}(L^{N4}\text{-}OH)]^{+}$ (**1**)/$(F_8)Fe^{II}$ (**3**) in THF at −60 °C. Equimolar mixture of **1** and **3** (blue) and $[(F_8)Fe^{III}-(O_2^{2-})-Cu^{II}(L^{N4}OH)]^{+}$ (**4**) (red).

imidazole−phenol containing Cu moiety to an iron-tetraphenyl porphyrinate (diagram below).[45]

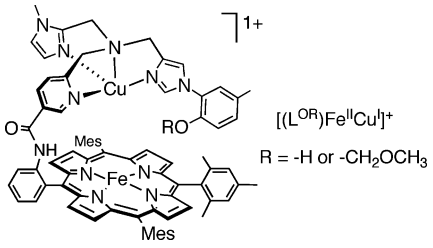

(1) UV−Vis Spectroscopy. Benchtop UV−vis spectroscopic changes for the oxygenation of a 1:1 mixture of $[Cu^{I}(L^{N4}OH)]^{+}$ (**1**) and $(F_8)Fe^{II}$ (**3**) are shown in Figure 3. The reduced mixture has absorptions at 422 and 542 nm at −60 °C in THF. Bubbling with dioxygen produced a stable dioxygen adduct with new spectral features at 417 (ϵ = 130 000 M^{-1} cm^{-1}), 540 (sh), and 560 (ϵ = 12 000 M^{-1} cm^{-1}) nm, significantly different features from those of the heme-only dioxygen adduct {λ_{max} = 416 and 536 nm for $(THF)(F_8)Fe^{III}-(O_2^{-})$ in THF; ν(O−O) = 1178 cm^{-1} and ν(Fe−O) = 568 cm^{-1}}[30,46] or the copper-only oxygenation product {λ_{max} = 541 and 613 nm from $[\{Cu^{II}(L^{N4}OH)\}_2(O_2^{2-})]^{2+}$ (**1b**), Figure 2}. This low-temperature stable dioxygen adduct can also be generated in acetonitrile (MeCN) solvent at −40 °C (Figure S5 in Supporting Information). Whereas the reduced mixture has different UV−vis features in MeCN from those in THF, probably because of the changes in the spin states of **3** (high-spin in THF but low-spin in nitriles at low temperatures),[30] the UV−vis spectra of the dioxygen adducts are essentially the same in both THF and MeCN (Figure 3 and Figure S5). We formulate this as $[(F_8)Fe^{III}-(O_2^{2-})-Cu^{II}(L^{N4}OH)]^{+}$ (**4**), on the basis of reaction stoichiometry (**1**/**3**:O_2 = 1:1, see Experimental Section and Supporting Information, Figure S6) and resonance Raman, EPR, and ^{1}H and ^{2}H NMR spectroscopies (vide infra). In contrast to dicopper peroxo species $[\{Cu^{II}(L^{N4}OH)\}_2(O_2^{2-})]^{2+}$ (**1b**), complex **4** is stable at low temperatures (below −60 °C) for several days without indication of decomposition. A similar heme−peroxo−copper complex $[(F_8)Fe^{III}-(O_2^{2-})-Cu^{II}(L^{N4}OMe)]^{+}$ (**5**) was also generated through oxygenation of the anisole complex $[Cu^{I}(L^{N4}OMe)]^{+}$ (**2**) and heme $(F_8)Fe^{II}$ (**3**) (i.e., 1:1 mixture) where the UV−vis features and thermal stability of **5** in solution are practically identical to those of **4**.

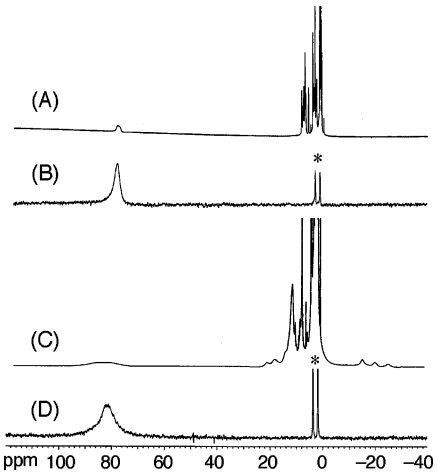

Figure 4. ^{1}H and ^{2}H NMR spectra of the oxygenation reaction of $[Cu^{I}(L^{N4}\text{-}OH)Cu^{I}]^{+}$ (**1**)/$(F_8)Fe^{II}$ (**3**) in THF at −60 °C. (A) ^{1}H and (B) ^{2}H NMR spectrum of an equimolar mixture of **1** and **3**. (C) ^{1}H and (D) ^{2}H NMR spectrum of $[(F_8)Fe^{III}-(O_2^{2-})-Cu^{II}(L^{N4}OH)]^{+}$ (**4**). * = solvent THF peaks.

(2) NMR Spectroscopy. The $[Cu^{I}(L^{N4}OH)]^{+}$ (**1**)/$(F_8)Fe^{II}$ (**3**)/O_2 reaction was also followed by low-temperature NMR spectroscopy. The positions of the pyrrole resonances in particular are very informative in assigning the oxidation and spin state of a heme complex.[47,48] Thus, deuterated iron porphyrinate $(F_8\text{-}d_8)Fe^{II}$ (**3-*d*$_8$**) was prepared to carry out ^{2}H NMR spectroscopy for unambiguous identification of the pyrrole chemical shift. In THF-d_8 at −60 °C, ^{1}H NMR spectra of the reduced **1**/**3** mixture exhibited paramagnetic peaks at 79 (pyrrole), 6.0 (*para*-phenyl), and 4.5 (*meta*-phenyl) ppm from the high-spin $(F_8)Fe^{II}$ (**3**) complex (with THF axial ligand),[30] as well as diamagnetic resonances from the copper(I) complex $[Cu^{I}(L^{N4}OH)]^{+}$ (**1**) (Figure 4A and 4B). Bubbling dry O_2 into a pre-cooled NMR tube containing **1** and **3** led to the formation of $[(F_8)Fe^{III}-(O_2^{2-})-Cu^{II}(L^{N4}\text{-}OH)]^{+}$ (**4**) with a downfield shifted broad pyrrole resonance at ∼83 ppm (Figure 4C and 4D). This observed position for a pyrrole chemical shift excludes the possibility of **4** being either (i) an iron-superoxide $(F_8)Fe^{III}-(O_2^{-})$ (δ = 8.9 ppm, −80 °C), (ii) a μ-peroxo-diheme $[(F_8)Fe^{III}]_2-(O_2^{2-})$ (δ = 17.5 ppm, −80 °C), (iii) the ferryl-oxo species $(F_8)Fe^{IV}$=O (δ = 3.5 ppm, −80 °C), or (iv) $(F_8)Fe^{III}$−OH (δ = 125 ppm

(44) This may be an important site for the proton translocation.
(45) Collman and co-workers[18,19] recently reported new binuclear heme−Cu ligands possessing an imidazole−phenol cross-link as well as an imidazole heme axial base. The corresponding metal complexes and their reaction chemistry, potentially important complementary systems, are not yet available.
(46) Kim, E.; Helton, M. E.; Wasser, I. M.; Karlin, K. D.; Lu, S.; Huang, H.-w.; Moënne-Loccoz, P.; Incarvito, C. D.; Rheingold, A. L.; Honecker, M.; Kaderli, S.; Zuberbühler, A. D. *Proc. Natl. Acad. Sci. U.S.A.* **2003**, *100*, 3623−3628.
(47) Walker, F. A. In *The Porphyrin Handbook*; Kadish, K. M., Smith, K. M., Guilard, R., Eds.; Academic Press: San Diego, CA, 2000; Vol. 5/NMR and EPR, pp 81−184.
(48) Walker, F. A.; Simonis, U. In *Biological Magnetic Resonance*: *NMR of Paramagnetic Molecules*; Berliner, L. J., Reuben, J., Eds.; Plenum Press: New York, 1993; Vol. 12; pp 133−274.

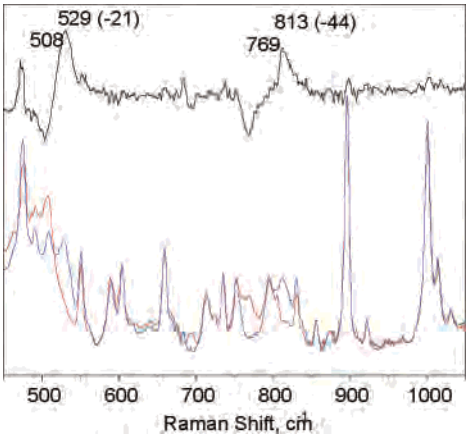

Figure 5. Resonance Raman spectra of $[(F_8)Fe^{III}-(O_2^{2-})-Cu^{II}(L^{N4}OH)]^+$ (**4**) formed by oxygenation with $^{16}O_2$ (blue) and $^{18}O_2$ (red). The difference spectrum of $^{16}O_2$ minus $^{18}O_2$ is shown in black. All spectra were obtained at ~90 K with excitation at 413 nm.

at −80 °C, δ = 110 ppm at −60 °C), each of which has characteristic NMR spectroscopic properties.[30] In fact, the pyrrole resonance is observed at the position close to those known for a high-spin Fe^{II} heme (e.g., 79 ppm from **3** at −60 °C, Figure 4B), rather than for a high-spin ferric heme (e.g., 110 ppm for $(F_8)Fe^{III}-OH$ at −60 °C). Additionally, Cu^{II}−ligand hydrogen resonances of **4** are observed at 21, 19, −16, −21, and −26 ppm for the $L^{N4}OH$ moiety (Figure 4C). These distinctive NMR features obtained for **4** (i.e., the position of pyrrole resonances and the observable Cu(II) ligand H resonances) are diagnostic of a strongly coupled (porphyrinate)$Fe^{III}-X-Cu^{II}$ complex (X = O_2^{2-} or O^{2-}), where antiferromagnetic coupling between high-spin Fe^{III} (d^5, S = 5/2) and Cu^{II} (d^9, S = 1/2) leads to a net S = 2 spin system.[1,23,25,49,50] The S = 2 assignment for **4** is further supported by EPR silent behavior (77 K, in THF frozen solution).

(3) Resonance Raman Spectroscopy. A 413-nm laser excitation within the porphyrin Soret absorption band of an MeCN frozen solution of $[(F_8)Fe^{III}-(O_2^{2-})-Cu^{II}(L^{N4}OH)]^+$ (**4**) produces porphyrin skeletal modes in the high-frequency region of the RR spectra consistent with a pentacoordinated high-spin ferric heme configuration.[51,52] Figure 5 compares the low-frequency RR spectra of **4** generated with $^{16}O_2$ and $^{18}O_2$. It reveals a $\nu(^{16}O-^{16}O)$ peroxo stretching vibration at 813 cm^{-1} which downshifted to 769 cm^{-1} upon $^{18}O_2$ substitution. In addition, a band at 529 cm^{-1} that shifts to 508 cm^{-1} with $^{18}O_2$ ($\Delta^{18}O_2$ = −21 cm^{-1}) is proposed to correspond to the ν(Fe−O) of the peroxide complex.[53]

Assignment of the O−O stretching vibrations to the dicopper complex $[\{(L^{N4}OH)Cu^{II}\}_2(O_2^{2-})]^{2+}$ (**1b**) was ruled out since the 413-nm laser excitation is not expected to provide resonance conditions for **1b** which presents absorption features at 541 and 613 nm (vide supra, Figure 2). Moreover, **1b** does not exist as a stable species under these experimental conditions, that is, oxygenation of $[Cu^I(L^{N4}OH)]^+$ (**1**) in MeCN solution at −40 °C immediately led to formation of $[Cu^{II}(L^{N4}O^-)]_2^{2+}$ (**1c**, Scheme 3) with absorption features at 518 and 793 nm. Although anionic mononuclear heme−peroxo species $[(F_8)Fe^{III}-(O_2^{2-})]^-$ could form through a reaction of $(F_8)Fe^{III}-(O_2^-)$ with a one-electron reductant (e.g.,cobaltocene),[24] its characteristic EPR signal at g = 4.3 was not observed in $[(F_8)Fe^{III}-(O_2^{2-})-Cu^{II}(L^{N4}OH)]^+$ (**4**) (vide supra). The mononuclear heme−peroxo species was also shown to display a sharp Soret absorption maximum at 435 nm,[24] in sharp contrast with the broad 417-nm Soret band associated with **4**. A homonuclear diheme−peroxo complex can also be ruled out since such species present pyrrole resonances at ~17 ppm in the NMR spectrum,[30,47] which is significantly different from what was found in **4** (83 ppm) (vide supra).

To test for possible hydrogen-bonding interactions between the cross-linked phenol and the bridging peroxide that may cause O−O bond weakening, RR studies on the anisole analogue $[(F_8)Fe^{III}-(O_2^{2-})-Cu^{II}(L^{N4}OMe)]^+$ (**5**) were carried out. As shown in Figure S7 (in Supporting Information), the ν(O−O) appeared at 815 cm^{-1} ($\Delta^{18}O_2$ = −46 cm^{-1}) as well as ν(Fe−O) at 528 cm^{-1} ($\Delta^{18}O_2$ = −22 cm^{-1}). These vibrational frequencies are nearly identical to those measured in the phenol complex $[(F_8)Fe^{III}-(O_2^{2-})-Cu^{II}(L^{N4}OH)]^+$ (**4**). On the basis of this comparison, we conclude that there is a negligible interaction between the peroxide group and the phenol moiety in **4**.

The observed ν(O−O) frequencies in $[(F_8)Fe^{III}-(O_2^{2-})-Cu^{II}(L^{N4}OH)]^+$ (**4**) and $[(F_8)Fe^{III}-(O_2^{2-})-Cu^{II}(L^{N4}OMe)]^+$ (**5**) are in fact very similar to those observed with other heme−peroxo−Cu complexes with a tetradentate Cu-chelate where the proximal phenol−imidazole moiety is absent (Table 3). In closest analogy is our previously described complex $[(F_8)Fe^{III}-(O_2^{2-})-Cu^{II}(TMPA)]^+$[23] and $[(P_{TMP-5MeTPA})Fe^{III}-(O_2^{2-})-Cu^{II}]^+$ (Chart 2), an X-ray structure of the latter

Table 3. Resonance Raman Data of Heme−Peroxo−Cu Complexes

complex	$\nu(^{16}O_2)$ ($\Delta(^{18}O_2)$) cm^{-1}	references
tetradentate Cu-ligand		
$[(F_8)Fe^{III}-(O_2^{2-})-Cu^{II}(L^{N4}OH)]^+$ (**4**)[a]	813 (−44)	This Work
$[(F_8)Fe^{III}-(O_2^{2-})-Cu^{II}(L^{N4}OMe)]^+$ (**5**)	815 (−46)	This Work
$[(F_8)Fe^{III}-(O_2^{2-})-Cu^{II}(TMPA)]^+$	808 (−46)	23
$[(^6L)Fe^{III}-(O_2^{2-})-Cu^{II}]^+$	788 (−44)	25
$[(L^{OH})Fe^{III}-(O_2^{2-})-Cu^{II}]^+$ [a]	799 (−47)	21
$[(L^{OMOM})Fe^{III}-(O_2^{2-})-Cu^{II}]^+$	801 (−46)	21
$[(P_{TMP-5MeTPA})Fe^{III}-(O_2^{2-})-Cu^{II}]^+$	790 (−44)	54
$[(P_{TPA})Fe^{III}-(O_2^{2-})-Cu^{II}]^+$	803 (−44)	55
$[(P_{5-MeTPA})Fe^{III}-(O_2^{2-})-Cu^{II}]^+$	793 (−42)	56
tridentate Cu-ligand		
$[(P_{TACN})Fe^{III}-(O_2^{2-})-Cu^{II}]^+$ [b]	758 (−18)	57
$[(F_8)Fe^{III}-(O_2^{2-})-Cu^{II}(L^{Me2N})]^+$	767 (−41), 752 (−46)	46
$[(^2L)Fe^{III}-(O_2^{2-})-Cu^{II}]^+$	747 (−40)	58

[a] Systems containing an imidazole−phenol cross-link. [b] Iron−porphyrinate moiety also has an imidazole axial base.

(49) Kopf, M. A.; Neuhold, Y. M.; Zuberbühler, A. D.; Karlin, K. D. *Inorg. Chem.* **1999**, *38*, 3093−3102.
(50) Nanthakumar, A.; Fox, S.; Murthy, N. N.; Karlin, K. D. *J. Am. Chem. Soc.* **1997**, *119*, 3898−3906.
(51) Nakamoto, K. *Infrared and Raman spectra of inorganic and coordination compounds*, 5th ed.; Wiley-Interscience: New York, 1997; Vol. Part B, pp 149−154, 336−342.
(52) Burke, J. M.; Kincaid, J. R.; Peters, S.; Collman, J. P.; Spiro, T. G. *J. Am Chem. Soc.* **1978**, *100*, 6083−6088.
(53) Variations in ν(Fe−O) in heme−peroxo−Cu complexes will be described elsewhere.

Chart 2

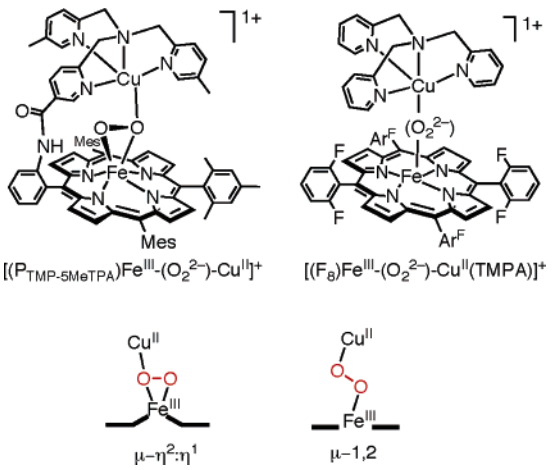

was recently determined,[54] revealing an asymmetric μ-η^2:η^1 peroxide bridge (i.e., η^2 to Fe and η^1 to Cu, Chart 2).

From the similarities of the UV−vis and RR spectra of **4**, **5**, [(F$_8$)Fe^{III}−(O$_2^{2-}$)−Cu^{II}(TMPA)]$^+$ [23] and [(P$_{TMP-5MeTPA}$)-Fe^{III}−(O$_2^{2-}$)−Cu^{II}]$^+$ (Chart 2), one might be tempted to hypothesize that all these peroxo complexes adopt a μ-η^2:η^1 peroxo binding mode. However, this asymmetric geometry with regard to the O−O bond is expected to result in a splitting of the ν(^{16}O−^{18}O) in RR experiments carried out with scrambled $^{16/18}$O-isotope. Such experiments were not reported with [(P$_{TMP-5MeTPA}$)Fe^{III}−(O$_2^{2-}$)−Cu^{II}]$^+$,[55] but with [(F$_8$)Fe^{III}−(O$_2^{2-}$)−Cu^{II}(TMPA)]$^+$ [23] and [(P$_{TPA}$)Fe^{III}−(O$_2^{2-}$)−Cu^{II}]$^+$ [55] (which is closely related to [(P$_{TMP-5MeTPA}$)Fe^{III}-(O$_2^{2-}$)−Cu^{II}]$^+$); the frozen solution RR results were consistent with a symmetric coordination of the peroxide group.[23] Thus, we consider that a symmetric μ-1,2 peroxo bridging geometry (Chart 2) in **4**, **5** and [(F$_8$)Fe^{III}−(O$_2^{2-}$)−Cu^{II}-(TMPA)]$^+$ is possible and we speculate that [(P$_{TMP-5MeTPA}$)-Fe^{III}−(O$_2^{2-}$)−Cu^{II}]$^+$ may adopt a different structure in the crystalline state versus in solution.

As shown in Scheme 1 (Introduction), the O−O bond cleavage at the heme a_3−Cu$_B$ binuclear center in C*c*O occurs by utilizing electrons provided from the metal centers and possibly the cross-linked phenol cofactor.[1,7] To induce such chemistry in **4**, other factors (besides number of electrons available) seem to be required; these could be extra protons or water molecules,[8] a heme axial base, or proper redox tuning for the metal centers.

Summary and Conclusion

We have studied the dioxygen chemistry of C*c*O Cu$_B$ model complexes [Cu^I(L^{N4}OH)]$^+$ (**1**) and [Cu^I(L^{N4}OMe)]$^+$ (**2**) in the absence and the presence of an iron-porphyrinate (F$_8$)Fe^{II} (**3**). These systems provide new copper−dioxygen and heme/Cu/O$_2$ chemistry with possible relevance to the imidazole−phenol cross-link in the O$_2$-reduction chemistry in the C*c*O active site. Different effects of the imidazole−phenol moiety were observed comparing Cu^I/O$_2$ and Cu^I/Fe^{II}/O$_2$ reactions, where at low temperatures, the cross-linked phenol group rapidly reacts to protonate the dicopper(II)−peroxo species, but it does not react with a heme−peroxo−Cu moiety. The fast **1**/O$_2$ reaction was investigated by stopped-flow kinetics, while low-temperature stable [(F$_8$)-Fe^{III}−(O$_2^{2-}$)−Cu^{II}(L^{N4}OH)]$^+$ (**4**) was studied by benchtop UV−vis, NMR, EPR, and RR spectroscopies.

When [Cu^I(L^{N4}OH)]$^+$ (**1**) reacts with dioxygen, the O$_2$-binding behavior of **1** is very similar to that of [Cu^I(TMPA)-(RCN)]$^+$, in which a transient 1:1 copper−dioxygen adduct [Cu^{II}(L^{N4}OH)(O$_2^-$)]$^+$ (**1a**) forms prior to formation of a 2:1 Cu$_2$O$_2$ adduct [{Cu^{II}(L^{N4}OH)}$_2$(O$_2^{2-}$)]$^{2+}$ (**1b**). Despite the fact that **1** and [Cu^I(TMPA)(RCN)]$^+$ have essentially the same Cu$^{II/I}$ redox-potentials, a much smaller equilibrium constant for O$_2$-binding to [Cu^I(L^{N4}OH)]$^+$ (**1**) is observed compared to that in the [Cu^I(TMPA)(RCN)]$^+$/O$_2$ reaction. This is probably due to the less favorable steric environment caused by the ligand architecture of L^{N4}OH. The peroxo complex **1b** is also a transient species, and it thermally transforms to a phenolate−Cu(II) dimeric complex [Cu^{II}-(L^{N4}O$^-$)]$_2^{2+}$ (**1c**) with proton donation from the phenol of the imidazole−phenol moiety. Thus, the neighboring imidazole−phenol moiety strongly affects the μ-1,2-peroxo dicopper(II) complex.

The oxygenation product of **1** in the presence of a heme complex (F$_8$)Fe^{II} (**3**) is completely different from the copper-only/O$_2$ chemistry, where a low-temperature stable O$_2$ adduct [(F$_8$)Fe^{III}−(O$_2^{2-}$)−Cu^{II}(L^{N4}OH)]$^+$ (**4**) is generated. Complex **4** is an S = 2 system with a bridging peroxide ligand which mediates antiferromagnetic coupling between high-spin iron(III) and copper(II). A very similar (in spectroscopic properties and thermal stability) heme−peroxo−Cu complex [(F$_8$)Fe^{III}−(O$_2^{2-}$)−Cu^{II}(L^{N4}OMe)]$^+$ (**5**) can be generated by utilizing the anisole compound [Cu^I(L^{N4}OMe)]$^+$ (**2**), thus indicating that the cross-linked phenol moiety in [(F$_8$)Fe^{III}−(O$_2^{2-}$)−Cu^{II}(L^{N4}OH)]$^+$ (**4**) does not interact with the peroxide. Resonance Raman spectroscopy further supports this view, where the observed ν(O−O) values from **4** and **5** are within a few cm^{-1} to that for [(F$_8$)Fe^{III}−(O$_2^{2-}$)−Cu^{II}-(TMPA)]$^+$ where the cross-linked phenol is absent. Preliminary experiments with the warming of **4** from −60 °C do not reveal phenoxyl radical nor Fe^{IV}=O formation products which might be expected if a biomimetic O−O cleavage reaction in **4** occurred. Yet, the fact that a stable heme−peroxo−copper species can be generated even in the presence of an imidazole−phenol group (i.e., possible electron/proton donor source) in close proximity provides new opportunities for studies probing key factors that can trigger the reductive O−O cleavage in C*c*O model compounds.

Acknowledgment. This work was supported by the National Institutes of Health (K.D.K (GM 60353 and

(54) Chishiro, T.; Shimazaki, Y.; Tani, F.; Tachi, Y.; Naruta, Y.; Karasawa, S.; Hayami, S.; Maeda, Y. *Angew. Chem., Int. Ed.* **2003**, *42*, 2788−2791.
(55) Sasaki, T.; Nakamura, N.; Naruta, Y. *Chem. Lett.* **1998**, 351−352.
(56) Naruta, Y.; Sasaki, T.; Tani, F.; Tachi, Y.; Kawato, N.; Nakamura, N. *J. Inorg. Biochem.* **2001**, *83*, 239−246.
(57) Collman, J. P.; Herrmann, P. C.; Boitrel, B.; Zhang, X.; Eberspacher, T. A.; Fu, L.; Wang, J.; Rousseau, D. L.; Williams, E. R. *J. Am. Chem. Soc.* **1994**, *116*, 9783−9784.
(58) Kim, E.; Shearer, J.; Lu, S.; Moënne-Loccoz, P.; Helton, M. E.; Kaderli, S.; Zuberbühler, A. D.; Karlin, K. D., *J. Am. Chem. Soc.* **2004**, *126*, 12716−12717.

GM28962), P.M.-L (GM18865)), and the Swiss National Science Foundation (A.D.Z).

Supporting Information Available: Kinetics studies (sampling information, results, Van't Hoff plot, time-dependent UV−vis spectra, Eyring plot), UV−vis spectra of the **1**/**3**/O_2 reaction in MeCN, O_2-titration (UV−vis) of **1**/**3**, and low-frequency RR spectra of **5**. The material is available free of charge via the Internet at http://pubs.acs.org.

IC048907B